

Electron-electron interaction and electron-hole asymmetry in bilayer graphene

K. Zou,¹ X. Hong,^{1,2} and J. Zhu^{1,3}

¹*Department of Physics, The Pennsylvania State University, University Park, PA 16802*

²*Department of Physics and Astronomy, University of Nebraska-Lincoln, Lincoln, NE 68588*

³*The Materials Research Institute, The Pennsylvania State University, University Park, PA 16802*

(Dated: Feb. 2, 2011)

We report precision measurements of the effective mass m^* in high-quality bilayer graphene using the temperature dependence of the Shubnikov-de Haas oscillations. In the density range of $0.7 \times 10^{12}/\text{cm}^2 < n < 4.1 \times 10^{12}/\text{cm}^2$, both the hole mass m_h^* and the electron mass m_e^* increase with increasing density, demonstrating the hyperbolic nature of the bands. The hole mass m_h^* is approximately 20-30% larger than the electron mass m_e^* . Tight-binding calculations provide a good description of the electron-hole asymmetry and yield an accurate measure of the inter-layer hopping parameter $v_4 = 0.063$. Both m_h^* and m_e^* are substantially suppressed compared to single-particle values, providing clear and unprecedented evidence for the strong renormalization effect of electron-electron interaction in the band structure of bilayer graphene.

PACS numbers: 73.43.Qt, 73.20.At, 71.70.Gm.

Bilayer graphene may be a technologically important material in electronics and photonics due to its tunable band gap. The fundamental property that underpins such applications—its band structure—has been the subject of many recent theoretical [1–4] and experimental studies using angle-resolved photoemission spectroscopy [5], infrared and Raman measurements [6–8] and compressibility measurements [9, 10]. On a single particle level, the band structure of bilayer is thought to be well described by a tight-binding Hamiltonian [2, 3] with a few leading order Slonczewski-Weiss-McClure parameters, i.e., γ_0 , γ_1 , γ_3 and γ_4 . Experimental knowledge of these hopping parameters in bilayer varies, with $\gamma_1 = 0.40$ eV fairly accurately known [7, 8] and the rest to a much less degree. For example, experimental values of γ_4 , which controls the band asymmetry, range from 0.11-0.19 eV [6–9].

Meanwhile, electron-electron interactions in single-layer and bilayer graphene are predicted to be strong and peculiar. Interesting collective states emerge in a magnetic field [11, 12]. The many-body corrections to Fermi liquid parameters such as the compressibility κ and the effective mass m^* are expected to be substantial already at currently accessible densities [13–15]. These renormalization effects are related to, but also quantitatively different from those observed in conventional two-dimensional electron gases (2DEGs) [16, 17], due to the chirality of single and bilayer graphene [14]. For example, instead of an enhancement [17], the effective mass of bilayer graphene is predicted to be increasingly suppressed at lower carrier densities [14]. No experimental evidence of such renormalization effect has been reported so far.

In this letter, we report the measurements of the effective mass m^* in bilayer graphene samples for a wide range of carrier densities using high-quality Shubnikov-de Haas (SdH) oscillations. The inter-layer hopping parameter γ_4 is determined to be $\gamma_4 = 0.063(1)\gamma_0$ with the highest accuracy reported so far. The magnitude and

density dependence of m^* deviate from tight-binding calculations and reveal strong evidence of electron-electron interaction. m^* is suppressed by 30-40% comparing to its non-interaction values.

Bilayer graphene flakes are exfoliated onto 290 nm SiO₂/Si wafers from highly ordered pyrolytic graphite and identified by optical microscope and Raman spectra. They are further confirmed by their quantum Hall sequence. Conventional electron-beam lithography is used to pattern the flakes into Hall bars. Transport measurements are carried out in a He⁴ system using standard low-frequency lock-in technique. The field effect mobility $\mu_{\text{FE}} = (1/e)(d\sigma/dn)$ of our pristine bilayer graphene ranges from 3 000-12 000 cm²/Vs. Data from two samples (A and B) are presented in this paper.

In Fig. 1, we plot the sheet conductance σ vs. the back-gate voltage V_{bg} of sample A at selected temperatures between 15 K–250 K. At 15 K, the mobility μ_{FE} of sample A is approximately 4 800 cm²/Vs for holes and 3 100 cm²/Vs for electrons. Sample B has a higher mobility of 6 300 cm²/Vs for holes and 6 800 cm²/Vs for electrons. The conductance of bilayer graphene samples shows a variety of temperature dependence, depending on the carrier density and mobility. Near the charge neutrality point, all our samples show an insulating-like T -dependence ($d\sigma/dT > 0$), as shown in Fig. 1. This behavior is due to the thermal excitation of carriers out of electron-hole puddles, as demonstrated in Ref. [18]. As the carrier density increases, $d\sigma/dT$ eventually becomes negative (metallic) in the highest-quality samples. This trend is shown by the hole branch in Fig. 1(a) and (b), where the crossover density is approximately $n_h = 2.1 \times 10^{12}/\text{cm}^2$. For samples with lower mobilities, the insulating-like T -dependence persists to high densities, an example of which is given by the electron branch in Fig. 1(b).

This complex behavior is in contrast to that of single-

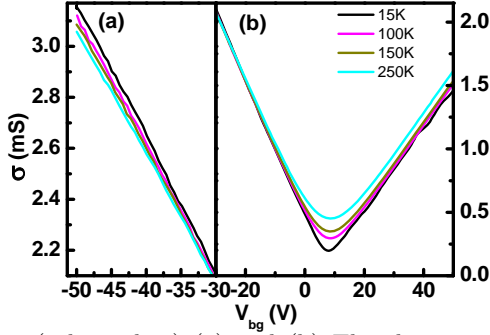


FIG. 1. (color online) (a) and (b) The sheet conductance $\sigma(V_{bg})$ of sample A. From top to bottom: $T = 15, 100, 150, 250$ K in (a) and in reverse order in (b). The charge neutrality point is at $V_{bg} = 7$ V.

layer graphene, where a metallic-like temperature dependence dominates over a wide range of densities due to phonon scattering [19–21]. The qualitative features of our data are consistent with the model proposed in Ref. [22], where $\sigma(T)$ combines metallic and insulating trends arising from the conduction of the majority and minority carriers respectively. The true metallic T -dependence of a bilayer graphene two-dimensional electron gas emerges only in high quality samples and/or at high carrier densities. In Fig. 1, the different T -dependence of the two carriers in the same sample points to an intrinsic electron-hole (e-h) asymmetry of bilayer graphene, which we further examine below.

To probe the band structure of bilayer graphene, we measure the effective mass m^* as a function of the carrier density using SdH oscillations. This technique is well established in 2DEGs but require high-quality oscillations to reliably extract m^* . Figure 2(a) shows the SdH oscillations $\rho_{xx}(B)$ of sample A at a high electron density $n_e = 3.26 \times 10^{12}/\text{cm}^2$ and varying temperatures. The oscillations have an early onset, appear sinusoidal and free of beating. Its amplitude $\delta\rho_{xx}$ is given by [23]:

$$\frac{\delta\rho_{xx}}{\rho_0} = 4\gamma_{th}\exp\left(-\frac{\pi}{\omega_c\tau_q}\right); \gamma_{th} = \frac{2\pi^2 k_B T / \hbar\omega_c}{\sinh(2\pi^2 k_B T / \hbar\omega_c)} \quad (1)$$

where $\omega_c = eB/m^*$ is the cyclotron frequency, τ_q is the quantum scattering time and γ_{th} the thermal factor.

As shown in Fig. 2(a), $\delta\rho_{xx}$ increases with increasing B and decreasing T . Its T -dependence provides a direct measure of m^* whereas the B -dependence is controlled by both m^* and τ_q . At each carrier density, the low-field $\delta\rho_{xx}(T, B)$ data, i.e., before the onset of the quantum Hall effect, is fit to Eq. 1 with two fitting parameters m^* and τ_q . The simultaneous fitting of m^* and τ_q allows us to accurately determine $\delta\rho_{xx}$, especially at low carrier densities, where the oscillations are few and a linear interpolation between peaks, as commonly done in the literature [17], cannot give the correct amplitude of $\delta\rho_{xx}$. Figure 2(b) shows $\rho_{xx}(B)$ data at $T = 10$ K and 40 K for a low hole density $n_h = 0.89 \times 10^{12}/\text{cm}^2$. Fittings to Eq. 1 are shown as dashed lines. Only the right values of m^*

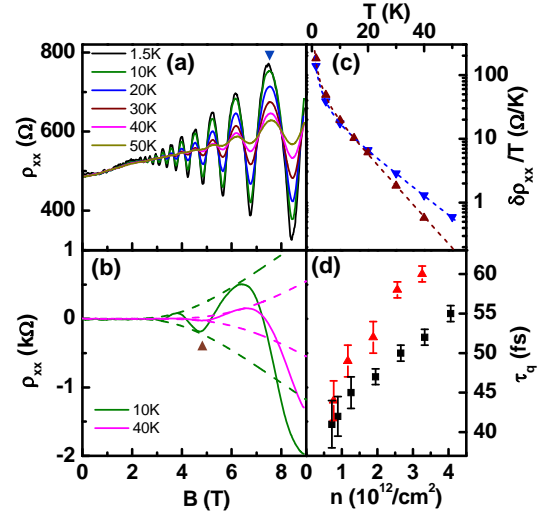


FIG. 2. (color online) (a) SdH oscillations $\rho_{xx}(B)$ at $T = 1.5$ – 50 K for $n_e = 3.26 \times 10^{12}/\text{cm}^2$. (b) $\rho_{xx}(B)$ at $T = 10$ K and 40 K for $n_h = 0.89 \times 10^{12}/\text{cm}^2$. Dashed lines are fittings with $\tau_q = 42$ fs and $m_h^* = 0.036m_e$. A smooth background has been subtracted. (c) $\delta\rho_{xx}/T$ vs. T in a semi-log plot for $n_e = 3.26 \times 10^{12}/\text{cm}^2$ at $B = 7.53$ T (down triangle in (a)) and for $n_h = 0.89 \times 10^{12}/\text{cm}^2$ at $B = 4.70$ T (up triangle in (b)). The symbols correlate. Dashed lines are fittings with $m_e^* = 0.041m_e$ (down triangles) and $m_h^* = 0.036m_e$ (up triangles). (d) τ_q vs. n for electrons (red triangles) and holes (black squares). All data in (a)–(d) are from sample A.

and τ_q can fit both the B -dependence and T -dependence of $\delta\rho_{xx}$ simultaneously.

In Fig. 2(c), we plot two examples of the measured $\delta\rho_{xx}/T$ vs. T in a semi-log plot for the two positions marked in Figs. 2(a) and (b) with down and up triangles respectively. Dashed lines are fittings generated with $m_e^* = 0.041m_e$ and $m_h^* = 0.036m_e$ respectively. They both fit very well. Overall, Eq. 1 provides an excellent description of the $\delta\rho_{xx}(T, B)$ data in the entire density range studied, with the uncertainty of m^* increasing from $0.0001m_e$ to $0.0015m_e$ from high to low densities. The global fitting procedure also ensures that the extracted m^* is filling factor independent and therefore represents the $B = 0$ limit, i.e., the band structure mass. This m^* is not directly comparable to m^* determined from cyclotron resonance measurements [24], as Coulomb interaction may manifest differently in these two cases [25]. A good illustration of this situation is the parabolic band material GaAs, where m^* determined from SdH oscillations embodies electron-electron (e-e) interaction [17] while its effect is forbidden in cyclotron resonance measurements by the Kohn theorem [26].

Using this method, we have determined m^* and τ_q for samples A and B in the density range of $0.7 < n < 4.1 \times 10^{12}/\text{cm}^2$ for electrons and holes. Both samples show oscillations of equally high quality and comparable τ_q . Figure 2(d) plots $\tau_q(n)$ of sample A for both carriers. Overall, τ_q increases with increasing density, ranging from 41 to 60 fs. These values correspond to a disorder broad-

ening $\Gamma = \hbar/2\tau_q = 5.5\text{-}8.0$ meV, which are similar to high-quality single and bilayer graphene samples [7, 23].

The results of m^* of samples A and B as a function of the carrier density n are plotted in Fig. 3(a). The error bars represent the fitting uncertainty in Fig. 2(c). The two samples agree very well with each other. In the density range studied, both m_e^* and m_h^* increase with increasing n , indicating the non-parabolic nature of the bands. This observation agrees with the compressibility measurements of Refs. [9, 10] and is also consistent with the observation of a constant m^* at yet lower densities [12]. The ratio of m_h^*/m_e^* is about 1.2-1.3, demonstrating a pronounced electron-hole asymmetry.

The above measurements of m^* provide an accurate means of determining the band structure of bilayer graphene and investigating the effect of e-e interaction. In the following analysis, we employ a tight-binding Hamiltonian following the notations of Refs. [3] and [7]:

$$H = \begin{pmatrix} V(n)/2 + \Delta & \phi & \gamma_1 & -v_4\phi^* \\ \phi^* & V(n)/2 & -v_4\phi^* & v_3\phi \\ \gamma_1 & -v_4\phi & -V(n)/2 + \Delta & \phi^* \\ -v_4\phi & v_3\phi^* & \phi & -V(n)/2 \end{pmatrix}. \quad (2)$$

Equation 2 is written in the basis of the four sublattices $(\Psi_{A1}, \Psi_{B1}, \Psi_{A2}, \Psi_{B2})$, where A1, A2 are the 2 stacked sublattices in layer 1 and 2 respectively. The nearest neighbor in-plane (A1-B1) hopping integral γ_0 is included in $\phi = \gamma_0(3/2k_y a - i3/2k_x a) = \hbar v_F(k_y - ik_x)$, where $a = 1.42\text{\AA}$ is the carbon-carbon distance and the momentum vector (k_x, k_y) originates from the K (K') point of the Brillouin zone. The Fermi velocity $v_F = (3/2)\gamma_0 a/\hbar$. $\gamma_1, v_3 = \gamma_3/\gamma_0$ and $v_4 = \gamma_4/\gamma_0$ represent the hopping integrals between two inter-layer sublattices A1-A2, B1-B2, and A1-B2 respectively. Δ is the on-site energy difference of A1 and B1, due to their stacking difference. $V(n)$ is the potential difference between the two layers and varies with the carrier density [7]. The eigenvalues of Eq. 2 produce the four low-energy bands of bilayer graphene. The two higher bands are neglected here since they are far above the Fermi level of our density range, $E_F \sim 30\text{-}120$ meV. The effective mass m^* of the lower bands is given by:

$$m^* = \frac{\hbar^2}{2\pi} \frac{dA(E)}{dE} \Big|_{E=E_F}, \quad (3)$$

where $A(E)$ is the k -space area enclosed by the contour of constant energy E . For $\gamma_3 = 0$, the contour is circular and Eq. 3 is simplified to $m^* = \hbar^2 k/(dE(k)/dk)$.

We diagonalize Eq. 2 and numerically compute m^* using Eq. 3. The effect of each parameter in Eq. 2 on m^* is summarized in table I, where +(-) means an increase of the parameter will increase (decrease) the value of m^* . $\gamma_0, \gamma_1, \gamma_3$ and $V(n)$ affect the overall magnitude of m_h^* and m_e^* , while v_4 and Δ control the e-h asymmetry.

In our calculations, we set $\gamma_1 = 0.40$ eV and $\Delta = 0.018$ eV, using results from infrared spectroscopy [7, 8]. The

TABLE I. The effect of tight-binding parameters on m^* and their values.

	γ_0	γ_1	γ_3	$V(n)$	v_4	Δ
m_h^*	-	+	+	+	+	+
m_e^*	-	+	+	+	-	-
value (eV)	3.43(1)	0.40 [†]	0		0.063(1)	0.018 [†]

[†].Reference [7].

inter-layer B1-B2 hopping energy γ_3 is set to zero due to its negligible effect in the density range considered here. The gate voltage-induced $V(n)$ is calculated following Eqs.(7)-(13) in Ref. [7]. The calculation details, as well as discussions on how the uncertainty of these parameters impact the results of γ_0 and v_4 can be found in Ref. [27].

The remaining adjustable parameters are γ_0 and v_4 . Fittings to both samples are given in Fig. 3(a). Both yield $v_4 = 0.063 \pm 0.001$. The value of γ_0 varies slightly from 3.419 eV in A to 3.447 eV in B, yielding an average $\gamma_0 = (3.43 \pm 0.01)$ eV. Our result of v_4 is consistent with the range of $v_4 \sim 0.04\text{-}0.06$ obtained previously [6-9], but has a much higher precision. This accurate knowledge of electron-hole asymmetry will be important to potential electronic and optical applications of bilayer graphene.

The above fitting does not include the in-plane next-nearest neighbor hopping integral γ_n [2], which also contributes to the electron-hole asymmetry of m^* , acting in the opposite direction of v_4 [28]. The value of γ_n is not well established. Including an additional diagonal term $-\gamma_n |\phi|^2 / \gamma_1^2$ in Eq. 2 [2], our calculations show that the effect of γ_n on v_4 can be represented by an empirical relation $v_4 = 0.063 + 0.037\gamma_n$, which can provide further correction to v_4 should the value of γ_n become known.

The fittings in Fig. 3(a) reveal an important trend of our data, i.e., the measured m^* increasingly drops below the calculated m^* as n decreases. This trend is consistently seen for both electrons and holes and in both samples. A perfect fit to both the high and low densities cannot be obtained by varying other parameters unless γ_1 is allowed to decrease from 0.4 eV to 0.3 eV, as shown by the short-dashed lines in Fig. 3(a). However, this solution is incompatible with the results of $\gamma_1 = 0.38\text{-}0.40$ eV obtained by infrared measurements [7, 8]. We therefore reject it and instead, interpret this trend as strong evidence of interaction induced renormalization of m^* . Indeed, a recent calculation in bilayer graphene predicts a monotonic suppression of m^* as a function of decreasing density [14]. First principle calculations also show that the inclusion of e-e interaction increases γ_0 from the non-interacting value of 2.7 eV to an interaction-modified value of 3.4 eV [4, 29, 30]. In our experiment, the suppression of m^* , its density dependence, and the fitting result of $\gamma_0 = 3.43$ eV all strongly point to the renormalization effect of e-e interaction on m^* .

The magnitude of this effect is illustrated in Fig. 3(b)

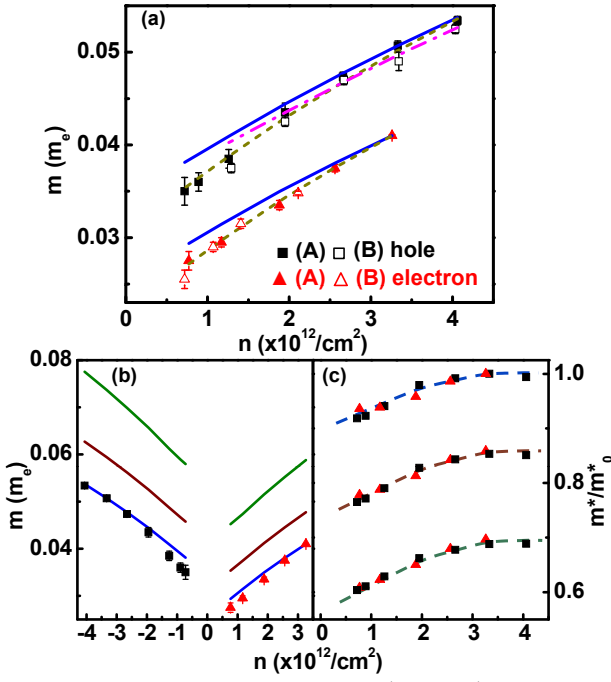


FIG. 3. (color online) (a) Measured m_h^* and m_e^* vs. n for samples A and B. The symbols are indicated in (a) and used in (a)-(c). Solid blue lines are fittings to sample A with $\gamma_0 = 3.419$ eV, $\gamma_1 = 0.40$ eV and $v_4 = 0.063$. The magenta dash-dotted line is a fitting to sample B with $\gamma_0 = 3.447$ eV, $\gamma_1 = 0.40$ eV and $v_4 = 0.063$. The yellow short dashed lines correspond to $\gamma_0 = 3.167$ eV, $\gamma_1 = 0.30$ eV and $v_4 = 0.063$. (b) A comparison of measured m^* and calculated m_0^* for sample A. From top to bottom: $\gamma_0 = 2.72$ (olive), 3.09 (wine), and 3.42 eV (blue). $\gamma_1 = 0.40$ eV, $v_4 = 0.063$ and $\Delta = 0.018$ eV for all traces. (c) The ratio m^*/m_0^* vs. n for sample A. From top to bottom: $\gamma_0 = 3.42, 3.09$, and 2.72 eV. Dashed lines are guide to the eye.

and (c), using sample A as an example. Here we calculate and plot three sets of m_0^* values using $\gamma_0 = 2.72, 3.09$, and 3.42 eV (corresponding to $v_F = 0.88, 1.0, 1.11 \times 10^6$ m/s respectively). These three values are the first principle non-interacting, intermediate and our fitting result of γ_0 respectively. The other parameters are fixed at values listed in Table I. Fig. 3(c) plots the ratio of measured m^* and the calculated m_0^* , m^*/m_0^* vs n for each γ_0 . The trend of decreasing m^*/m_0^* with decreasing density is seen in each case, with the magnitude of the suppression depending on the input value of γ_0 . Electrons and holes follow the same trend. When the first principle non-interacting value of $\gamma_0 = 2.72$ eV is used (bottom trace in Fig. 3(c)), the suppression of m^* is quite large, varying from 0.6 to 0.7 in the density range $0.7 < n < 4 \times 10^{12}/\text{cm}^2$. These observations provide the first experimental evidence of e-e interaction induced strong band renormalization effect in bilayer graphene. The quantitative input provided by our data should constrain and guide future calculations on this important subject, as the correct theory must capture both the magnitude and the density dependence of m^* .

To conclude, we report the measurement of effective

mass m^* in bilayer graphene over a wide range of electron and hole densities. Our results demonstrate a pronounced electron-hole asymmetry, from which we accurately determine the inter-layer hopping parameter v_4 in the tight-binding description of the band structure. The measured m^* is substantially suppressed compared to single-particle predictions; the discrepancy attributed to many-body effect. Our results provide critical experimental input to understand the effect of electron-electron interaction in this unique two-dimensional electron system.

We are grateful for discussions with M. Cohen, V. Crespi, M. Fogler, J. Jain, ZQ. Li and M. Polini. This work is supported by NSF CAREER grant no. DMR-0748604 and NSF NIRT grant no. ECS-0609243. The authors acknowledge use of facilities at the PSU site of NSF NNIN.

-
- [1] E. McCann, Phys. Rev. B **74**, 161403 (2006).
 - [2] M. Mucha-Kruczynski, E. McCann, and V. I. Fal'ko, Semicond. Sci. and Tech. **25**, 033001 (2010), and references therein.
 - [3] J. Nilsson *et al.*, Phys. Rev. B **78**, 045405 (2008).
 - [4] P. Gava *et al.*, Phys. Rev. B **79**, 165431 (2009).
 - [5] T. Ohta *et al.*, Science **313**, 951 (2006).
 - [6] L. M. Malard *et al.*, Phys. Rev. B **76**, 201401 (2007).
 - [7] L. M. Zhang *et al.*, Phys. Rev. B **78**, 235408 (2008).
 - [8] A. B. Kuzmenko *et al.*, Phys. Rev. B **80**, 165406 (2009).
 - [9] E. A. Henriksen and J. P. Eisenstein, Phys. Rev. B **82**, 041412 (2010).
 - [10] A. F. Young *et al.*, arXiv:1004.5556 (2010).
 - [11] Y. Zhao *et al.*, Phys. Rev. Lett. **104**, 066801 (2010).
 - [12] J. Martin *et al.*, Phys. Rev. Lett. **105**, 256806 (2010).
 - [13] S. V. Kusminskiy *et al.*, Phys. Rev. Lett. **100**, 106805 (2008).
 - [14] G. Borghi *et al.*, Solid State Comm. **149**, 1117 (2009).
 - [15] G. Borghi *et al.*, Phys. Rev. B **82**, 155403 (2010).
 - [16] G. Giuliani and G. Vignale, *Quantum Theory of the Electron Liquid* (Cambridge University Press, 2005).
 - [17] Y. Tan *et al.*, Phys. Rev. Lett. **94**, 016405 (2005).
 - [18] K. Zou and J. Zhu, Phys. Rev. B **82**, 081407 (2010).
 - [19] J. H. Chen *et al.*, Solid State Comm. **149**, 1080 (2009), and references therein.
 - [20] W. Zhu *et al.*, Phys. Rev. B **80**, 235402 (2009).
 - [21] K. Zou *et al.*, Phys. Rev. Lett. **105**, 126601 (2010).
 - [22] E. H. Hwang and S. Das Sarma, Phys. Rev. B **82**, 081409 (2010).
 - [23] X. Hong, K. Zou, and J. Zhu, Phys. Rev. B **80**, 241415 (2009).
 - [24] E. A. Henriksen *et al.*, Phys. Rev. Lett. **104**, 067404 (2010).
 - [25] K. Shizuya, Phys. Rev. B **81**, 075407 (2010); L. M. Zhang *et al.*, arXiv:1008.1418 (2010).
 - [26] W. Kohn, Phys. Rev. **123**, 1242 (1961).
 - [27] See supplementary material at <http://> for details of the calculation.
 - [28] γ_n does not lead to measurable effect in infrared measurements [7].
 - [29] P. E. Trevisanutto *et al.*, Phys. Rev. Lett. **101**, 226405 (2008).

(2008).

- [30] C.-h. Park *et al.*, Nano Letters **9**, 4234 (2009).